



A reproducible method to characterize the bulk morphology of cellulose nanocrystals and nanofibers by transmission electron microscopy

Cristina Campano · Ana Balea · Ángeles Blanco · Carlos Negro

Received: 19 December 2019 / Accepted: 31 March 2020 / Published online: 9 April 2020
© Springer Nature B.V. 2020

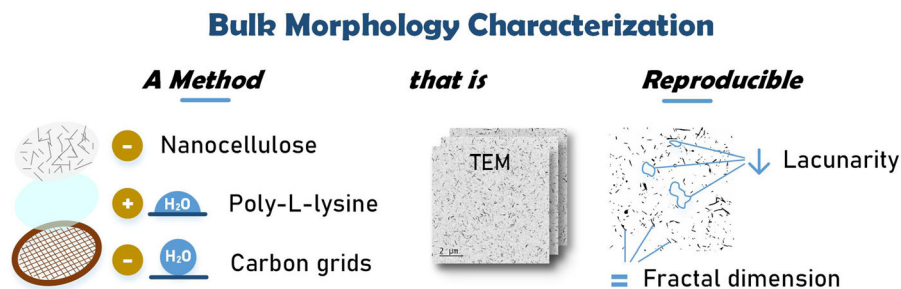
Abstract With the increased use of nanocelluloses as additives in many industrial applications, better characterization methods are needed to ensure their effectiveness. Transmission electron microscopy (TEM) is an appropriate image acquisition system to enable their morphological characterization. The use of TEM has typically been focused on determining the diameter and length of individual cellulose nanocrystals (CNCs) or nanofibers (CNFs), so different dispersion practices, such as sonication or the use of dispersants, are commonly applied to separate the particles. However, this study aims to improve the characterization of the bulk morphology of CNCs and CNFs by TEM, taking steps towards the determination of the aggregation/dispersion degree as well as the fibrillation degree of CNFs. TEM has been

investigated with two types of grids (holey and Formvar/carbon), three different fixing methods (Poly-L-Lysine, glow discharge and UV radiation) and the use of negative staining. Fractal dimension and lacunarity were used to quantify the reproducibility of the improved method. With the use of Poly-L-Lysine, the attachment of CNCs and CNFs particles on the TEM grids was ensured, due to the electrostatic interactions between negatively charged nanocelluloses and positively charged and hydrophilic Poly-L-Lysine surfaces. The low value of lacunarity, close to 0.3, shows a very high reproducibility of the methodology proposed. With this new approach, the state that the nanocelluloses have in suspension can be directly characterized by TEM.

Electronic supplementary material The online version of this article (<https://doi.org/10.1007/s10570-020-03138-1>) contains supplementary material, which is available to authorized users.

C. Campano · A. Balea · Á. Blanco · C. Negro (✉)
Department of Chemical Engineering and Materials,
Complutense University of Madrid, Avda. Complutense
S/N, 28040 Madrid, Spain
e-mail: cnegro@ucm.es

Graphic abstract



Keywords Transmission electron microscopy · Cellulose nanocrystals · Cellulose nanofibers · Poly-L-lysine · Lacunarity · Fractal dimension · Nanocellulose

Introduction

The superior mechanical and chemical properties of cellulose nanocrystals (CNCs) and nanofibers (CNFs) have been widely recognized during the last two decades opening a large range of high-end potential applications in different industrial sectors (Klemm et al. 2018). The effectiveness of the use of CNCs and CNFs is directly influenced by their three-dimensional structure or bulk morphology, including their shape, size, and aggregation/dispersion degree (Arias et al. 2015; Kaushik et al. 2015b). Thus, from an industrial point of view, it is essential to have reliable data on CNCs and CNFs bulk morphology, especially for quality control, toxicology assessment, research and development studies of new applications.

In the case of CNCs, ester sulfate groups formed at their surface after sulfuric acid hydrolysis enable their stabilization in water as colloidal suspensions (Araki 2013). However, colloidal stability can be easily destroyed either by a low surface charge density or by an increased ionic strength, promoting the aggregation of CNCs by attractive van der Waals interactions (Cherhal et al. 2015). Mohraz et al. (2004) proved that different CNCs aspect ratios leads to aggregates of different shapes, as observed by the values of fractal dimension. The different possible aggregation patterns of CNCs can affect the subsequent application in a significant way.

On the other hand, it has been proved that a high nanofibrillation degree of CNFs, determined with the

traditionally used gravimetric methodology, is not a guarantee of a highly efficient application of CNFs (Balea et al. 2016b). Hence, surface area and fiber dispersion have been demonstrated to be the most relevant parameters for many applications (Sanchez-Salvador et al. 2020). There is, therefore, a need to develop a method for the determination of nanofibrillation yield, which corresponds to a real interpretation of the surface area of the CNFs. Thus, though it is known that the bulk morphology of CNCs and CNFs is highly relevant, there is still lack of information regarding this issue.

The size and morphology of CNCs and CNFs can be accurately determined either by microscopy techniques, including transmission electron microscopy (TEM) (Brinkmann et al. 2016), cryo-TEM or atomic force microscopy (AFM) (Campano et al. 2017), or by scattering techniques such as polarized and depolarized light scattering (DLS and DDLS, respectively) and small- and wide-angle neutron or X-ray scattering (SANS, WANS, SAXS, and WAXS, respectively). In this context, TEM offers several advantages: it allows visualization of individual and aggregated particles, its resolution is well adapted for the imaging of nanocelluloses (NC), allowing rapid screening of a large population of particles, with tunable sampling (Brinkmann et al. 2016; Kaushik et al. 2015b). However, there are still some limitations associated with the use of TEM for the characterization of the three-dimensional structure or bulk morphology of either CNCs or CNFs (Table 1).

To ensure a proper characterization of these parameters, namely the description of the aggregation/dispersion degree of CNCs or the nanofibrillation degree of CNFs, one relevant factor must be considered: the distribution of particles must be representative in every image taken of the same sample. For this

Table 1 Limitations of the characterization of CNCs and/or CNFs morphology in the literature

Objective	NC	Technique	Method	Limitations	References
Individual Size	CNCs	TEM	Sonication or use of dispersing agents	Bulk morphology was disrupted	Kaushik et al. (2014); Stinson-Bagby et al. (2018)
	CNCs	TEM, AFM	Holey grids + UA ^a	Aggregation during drying	Kvien et al. (2005)
	CNCs/CNFs	TEM, AFM	Hydrophilic carbon grids	Measurement of individual CNCs/CNFs	Brinkmann et al. (2016), Chinga-Carrasco et al. (2011) and Elazzouzi-Hafraoui et al. (2007)
Aggregation	CNCs/CNFs	SANS, DLS	Variation of ionic strength, pH, surface charge, concentration	Aggregation was observed but aggregates were not described	Cherhal et al. (2015) and Fall et al. (2011)
	CNCs	SANS, TEM, AFM, DLS	Description of bulk morphology	Low reproducibility in images	Uhlig et al. (2016)
3D structure	CNCs-Pd	Cryo-TEM	Chiral deposition of Pd on well-dispersed CNCs	Position of Pd in CNCs and not the distribution of CNCs	Kaushik et al. (2015a)
	CNF-M	TEM	Glow-discharged grid + PTA ^b	Need of a glow discharge unit	Chen et al. (2015)

^aUA uranyl acetate

^bPTA phosphotungstic acid

purpose, the sample has to be fixed to the substrate, avoiding any type of modification or aggregation during sampling and drying.

Glow discharge has been considered to be the most efficient pretreatment to increase hydrophilicity of the TEM grids (Kaushik et al. 2015b). However, a glow discharge unit is needed, which is not typically present in common laboratories, and the conditions have to be optimized in each case. The use of Poly-L-lysine (PLL) has been proved to increase hydrophilicity of some substrates for microscopy observation, such as glass coverslips for cryo-electron microscopy (Kaech and Banker 2006) or mica for AFM (Yang et al. 2015). PLL has assured the attachment of NC samples on the substrates due to the electrostatic interactions between negatively charged NC and the positively charged PLL surfaces (Dulińska et al. 2006). Although the efficiency of PLL has been proved in many substrates (Dulińska et al. 2006; Xu et al. 2014), their use as fixing agent for TEM imaging has not apparently been reported.

In this study, a method is developed to ensure that the bulk morphology of nanocellulosic suspensions (CNCs and CNFs) is not altered in the course of the sampling process required for microscopic TEM image acquisition, with the ultimate objective of devising reproducible NC characterization strategies. In this way, some factors that typically limit the use of this technique to quantify the 3D conformation of nanoparticles could be removed, viz. the coffee ring effect, aggregation during drying and the effects of multiple layering. Thus, four different NC have been studied, considering several aspects that influence the acquisition process. Namely, the use of two different types of grid-one with holes and the other with a continuous layer-; the use of fixing agents -such as PLL, UV radiation and glow discharge-; and finally, the need for negative-staining of the grid deposited samples. To assess the reproducibility of the methods, we have measured fractal dimension and lacunarity on the images.

Fractal dimension is a very useful tool for estimating the irregularity or the roughness of ideal fractals

and natural objects which are not included in classical geometry. However, self-similar objects with identical fractal dimension can differ significantly in their textural appearance. While the fractal dimension quantifies how much space is occupied in an area, the so called lacunarity supplements fractal dimension with its ability to quantify how the space is occupied. In general, the larger the dispersion of gap sizes in the imaged texture, the higher the computed lacunarity (Reiss et al. 2016). Although these two parameters have been used before for the description of the textural appearance of very diverse samples, their use for the quantification of the reproducibility of a method has apparently not been reported before.

Materials and methods

Materials

Cotton linters, used as raw material for CNCs production, were supplied by Sigma Aldrich. Chemicals used for the reaction and characterization of the CNCs, namely H_2SO_4 and Copper (II) ethylenediamine, were also supplied by Sigma Aldrich (analytical reagent grade). Bleached softwood kraft fibers (*Pinus Radiate*), used as cellulosic source for CNFs production, were supplied by Celulosa Arauco y Constitución (Chile). 2,2,6,6-tetramethylpiperidin-1-oxyl (TEMPO)/sodium bromide (NaBr)/sodium hypochlorite (NaClO) system was used as chemical pretreatment to produce CNFs. Laboratory grade NaBr and 10% NaClO solution were purchased from PANREAC. TEMPO catalyst was supplied by Sigma Aldrich (analytical reagent grade). Poly-L-Lysine solution 0.1 wt% was obtained from Electron Microscopy Sciences.

Production of cellulose nanocrystals

Cellulose was subjected to acid hydrolysis with 64 wt% H_2SO_4 in a water bath at 45 °C for 45 min, with an acid to pulp ratio of 13.5 mL/g (Dufresne 2012). The reaction was then stopped by dilution of the reaction mixture by 10 times with distilled water and left to settle overnight. The sediment was washed under several cycles of centrifugation using a 3–16 L centrifuge supplied by JP Selecta S.A. (Barcelona, Spain) at $4500\times g$ for 15 min to remove excess acid.

This procedure was repeated until the supernatant became turbid. Finally, the suspension was dialyzed against distilled water using tubing membranes made of regenerated cellulose with a molecular weight cut-off of 12,000–14,000 Da, supplied by Medicell International Ltd. (London, UK), until the pH was close to neutral.

Production of cellulose nanofibers

Two types of CNFs were used for the experimentation: CNFs produced through TEMPO-mediated oxidation of the pulp and homogenization (CNF-T) and CNFs produced through mechanical refining of the pulp and homogenization (CNF-M). CNF-T were obtained by TEMPO-mediated oxidation with 5 mmol of NaClO per g of dry pulp at 25 °C and pH 10 (Saito et al. 2007). Once the pulp was oxidized, a cleaning process was performed through filtration steps with distilled water to reach a pH value around 7. CNF-M were produced by refining the pulp in a PFI mill at 20,000 revolutions according to the ISO standard 5264-2. Finally, both pulps were homogenized at 600 bars and 3 passes in the laboratory PANDA homogenizer manufactured by GEAS Niro Soavy (Parma, Italy).

Characterization of cellulose nanocrystals and cellulose nanofibers

Yields

The hydrolysis yield of CNCs was determined considering the dry mass of the produced CNCs and the dry mass of the initial pulp. The mass loss during hydrolysis contained two components: the hydrolyzed amorphous cellulose dissolved as glucose and the losses during the CNCs washing. Dissolved amorphous cellulose (DAC) was determined through the measurement of the chemical oxygen demand (COD) of the filtrated supernatant after dilution of the reaction mixture. The Nanocolor® COD 1500 test method (Macherey–Nagel GmbH) was used to determine the amorphous cellulose and through a Thermo Aquamate UV–Vis spectrophotometer, the value of COD was obtained. Assuming all organic material corresponds to cellulose, DAC can be determined through the equation: $DAC\ (mg/L) = COD/1.185$. This relationship was developed by Wang et al. (2012) through calibration with Avicel. Hydrolysis losses were

determined through the calculation: 100%—DAC—hydrolysis yield (Campano et al. 2017).

The nanofibrillation yield of CNFs was determined by centrifugation of 0.1 wt% of diluted suspensions at $4500\times g$ for 30 min. The nanofibrillated fraction was isolated in the supernatant, and the yield was calculated as the relation between dry solids in the supernatant and total dry solids in the sample.

Transmittance

Transmittance of the CNFs suspensions (0.1 wt%) was measured between 800 and 400 nm of wavelength range using a Cary 50 Conc UV–visible spectrophotometer (Varian Australia PTI LTD, Victoria, Australia).

Polymerization degree

Polymerization degree (PD) was determined from intrinsic viscosity (η) of the cellulosic suspension dissolved in cupri-ethylene-diamine solution according to ISO 5351. The following equation was used to correlate η with PD: $\eta = 0.42\cdot PD$ valid for $PD < 950$ and $\eta = 2.28\cdot PD^{0.76}$ valid for $PD > 950$ (Henriksson et al. 2008).

Crystallinity index

X-ray diffraction (XRD) analysis was carried out in order to determine the crystallinity index (Cr.I). Spectra were obtained with a Philips X'Pert MPD X-Ray diffractometer with an autodivergent slit fitted with a graphite monochromator using Cu-K α radiation operated at 45 kV and 40 mA. The XRD patterns were recorded from 3 to 80° at a scanning speed of 1.5°/min. Cr.I was determined using Segal's method (Segal et al. 1959) through the Eq. (1).

$$Cr.I(\%) = \frac{I_{002} - I_{am}}{I_{002}} \times 100 \quad (1)$$

where I_{002} is the intensity of the 002 plane at $2\theta = 22.5^\circ$ and I_{am} is the intensity of the amorphous scatter at $2\theta = 18^\circ$.

Zeta-potential

Samples were prepared at a concentration of 0.05 wt% and pH 7.3 mL of sample were added into the cuvette.

The cell was then immersed into the cuvette to then place it inside the chamber. Zeta potential was measured with a ZetaPlus analyzer supplied by Brookhaven Instruments Corporation (New York, USA). The result was the average value of at least 5 measurements.

Cationic demand

Cationic demand (CD) was measured by colloidal titration of 10 mL of 0.05–0.1 wt% diluted suspensions with N-polyDADMAC 0.001 N on a Mütek PCD04 particle charge detector (BTG Instruments GmbH, Herrsching, Germany).

Sulfate ester groups

Sulfate ester groups for CNCs were determined through elemental microanalysis using a LECO CHNS-932. Sample was dried and milled before analysis. This technique is reported to have a level of detection of $< 0.20\%$.

Carboxylic groups

The amount of carboxylic groups of CNFs suspensions, to evaluate the oxidation degree achieved after TEMPO-mediated oxidation, was determined by conductimetric titration according to Balea et al. (2016a) and calculated based on the method developed by Habibi et al. (2006).

Transmission electron microscopy

Samples were observed with a JEOL JEM 1400 plus TEM device, operated at 100 kV accelerating voltage. The CCD camera was an Orius SC200, manufactured by Gatan (Pleasanton, USA), of 2048×2048 pixels, and with a pixel size of 7.4 microns. Tests were carried out at the Spanish National Centre of Electronic Microscopy (CNME). At least 10 images were taken for each grid, considering areas far from each other and trying to represent the whole grid surface.

Different protocols were tried with four different NC. On the one hand, CNCs samples were diluted to a final concentration of 0.01 wt%, and tests were carried out with both the untreated sample (CNC-0) and with the sample submitted to 3 min of high intensity sonication (CNC-US), using a digital ultrasonic

processor UP200St from Hielscher Ultrasonics GmbH (Teltow, Germany). On the other hand, CNF-T and CNF-M were diluted to a final concentration of 0.005 wt% and 0.001 wt%, respectively, and then submitted to 3 min of high intensity sonication, using the previously described device. These concentrations were selected based on preliminary tests, with the main objective of minimizing the effect of dilution on the bulk morphology of the NC, but allowing a representative observation of the nanoparticles.

In all cases, 10 μL of sample were deposited on a grid placed on filter paper (in order to rapidly remove the excess moisture of the sample), and left to air-dry without any movement to avoid aggregation during handling. The volume of the sample used to prepare TEM samples was optimized to avoid multiple layering and re-concentration of the sample. Then, grids were placed into an oven at 60 $^{\circ}\text{C}$, to completely remove the water. The micropipette had an output diameter of 0.68 mm and since the CNCs and CNF-T aggregates were a maximum of 0.2 mm the samples were not disrupted by the pipette. Although fibers present in CNF-M are 1.3 mm long, their diameter is small enough to allow the sample to pass through the pipette tip.

Type of grid

200-mesh copper grids were considered in this study using two different covering configurations. The first one was an emulsion prepared following a standard procedure (Reichelt et al. 1977), consisting of a 0.1% solution of cellulose acetobutyrate (Triafol) in ethyl acetate containing a few drops of glycerin. The grids were covered with this solution and then, they were strengthened by a coating of carbon. These holey grids are often used in TEM analysis due to their simplicity in preparation as well as their low relative cost (Kaushik et al. 2015b).

The Formvar/carbon type of grid was considered with the purpose of easing the subsequent image analysis and, eventually, to automate it. From the most used grid coverages, the one with Formvar/carbon presents better quality/cost ratio (Kaushik et al. 2015b), so this type was included in this study. They were acquired from Electron Microscopy Sciences. These grids were covered with 10 nm Formvar and stabilized with 1 nm evaporated carbon film.

Fixing agents

In order to improve the homogeneity of the sample over the whole grid surface, the grid hydrophilicity had to be improved. Three different methods were used for this purpose: first, 20 μL of a 10% solution of PLL were deposited on the grids placed on filter paper, and left to dry before sample addition. The PLL volume was selected on the basis of preliminary tests. Secondly, grids were submitted to 2 h of UV radiation before sample application. And thirdly, a glow discharge was applied on the TEM grids, with a high vacuum coater EM ACE600 supplied by Leica (Barcelona, Spain) for 30 s under reduced air pressure (0.1–1.0 mbar). The protocol used for this technique was chosen based on bibliographic data (Ogawa and Putaux 2019).

Negative-staining

All prepared TEM samples were stained negatively, after observation with optical microscope, employing 2% uranyl acetate (Brinkmann et al. 2016). Grids were in contact with the staining agent for 30 s and the excess was removed with filter paper. Then, they were air-dried.

Image analysis

The assessment of the homogeneity of the micrographs was carried out using the ImageJ software package. Images were processed following a procedure adapted from Young and Morrison (2018). Briefly, they were converted to 8-bit and the frequency of dots in the background was reduced with the application of a bandpass filter and a background subtraction. Next, brightness and contrast were adjusted manually to highlight the sample present in the image. An unsharp mask filter was then run to further increase contrast and the images were binarized using a threshold. The *Close* plugin was then conducted to connect every two dark pixels that are separated by less than 2 pixels. Finally, with the plugin *Remove outliers*, the dark outlier pixels were replaced by the median pixels in the surrounding area if they deviated by more than a certain value. An example of the result of the image treatment is shown in Fig. S1.

Fractal dimension and lacunarity were determined running the plugin *FracLac* on the processed images.

The box counting method was used, setting 12 cycles in each image with a random grid design.

Results and discussion

Nanocellulose characterization

Results of the characterization made for CNC-0, CNC-US, CNF-T and CNF-M are shown in Table 2. As it can be observed, the cotton pulp used for CNCs production was mostly of a crystalline nature, achieving 38% of DAC after hydrolysis and a high Cr.I of 99%, indicating that the CNCs sample is almost completely crystalline. This fact permitted a suspension of 1.2% of concentration. On the other hand, a low proportion of sulfate ester groups (close to 170 mmol/kg) was observed in the sample which resulted in a zeta potential of -24 mV. Sulfate ester groups typically confer certain stability to CNCs suspensions, avoiding up to a certain point, the aggregation through hydrogen bonding (Beck et al. 2015). According to Riddick (1968), when the average zeta potential value of a suspension is between -16 and -30 mV, which is the case here, the sample is on the threshold of unstable dispersion. Thus, the CNCs suspension obtained right after acid hydrolysis could have some aggregates in suspension. This fact was found very useful in this study to assess the effectiveness of the different TEM sample preparation methods considered. In order to obtain a much more disperse sample to compare with the original one, high intensity sonication of a diluted suspension was used.

Although both CNFs were produced from the same virgin pulp and with the same mechanical

defibrillation treatment, the characterization results were quite different as a consequence of the different pretreatments carried out prior to the homogenization step. The carboxylic groups of CNF-M were 0.186 mmol/g, while for CNF-T they were 1 mmol/g due to the TEMPO-mediated oxidation of the pulp. The presence of a higher proportion of carboxylic groups in the pulp increases the repulsive forces between fibers and contributes to an easier defibrillation during the homogenization step (Balea et al. 2016b). Consequently, both nanofibrillation yield (95.7% for CNF-T vs. 7.3% for CNF-M) and transmittance of the CNF-T suspension (up to 90% for CNF-T) were higher. It is well known that CD represents the anionic nature of the CNFs while zeta potential indicates the stability of suspensions related to the repulsion degree between fibers. As a consequence of the TEMPO-mediated oxidation treatment, high CD and zeta potential (absolute value) were obtained for CNF-T, indicating that the suspension has a high electro-steric stability. On the contrary, the sample CNF-M gave the lowest zeta potential value (-18.5 mV) due to the lower fibrillation degree and charge of the hydroxyl groups.

The PD of CNF-T was lower than that of CNF-M (170 vs. 1200), which confirmed the break of the cellulose chains caused by the nanofibrillation process. The significantly different properties that both CNFs samples present, is the reason they were chosen for this study with the purpose of proving the feasibility of the TEM sample preparation methods proposed.

Table 2 Results of the characterization of the nanocellulose samples used in this study

Property	CNCs	CNF-T	CNF-M
Yield (%)	48.5 ± 0.2	95.7 ± 1.3	7.3 ± 0.3
DAC (%)	38.2 ± 1.5	–	–
PD	240 ± 5	170 ± 2	1200 ± 10
Cr.I (%)	99 ± 1	–	–
Zeta potential (mV)	-23.9 ± 1.4	-41.3 ± 0.9	-18.5 ± 0.5
Cationic demand ($\mu\text{eq/g}$)	133.0 ± 0.5	838.5 ± 0.3	50.5 ± 0.1
Sulfate ester groups (mmol/g)	0.168 ± 0.011	–	–
Carboxylic groups (mmol/g)	–	1.099 ± 0.111	0.186 ± 0.002
Transmittance 400 nm (%)	–	90.5 ± 0.6	13.9 ± 0.3
Transmittance 800 nm (%)	–	95.6 ± 0.7	1.5 ± 0.1

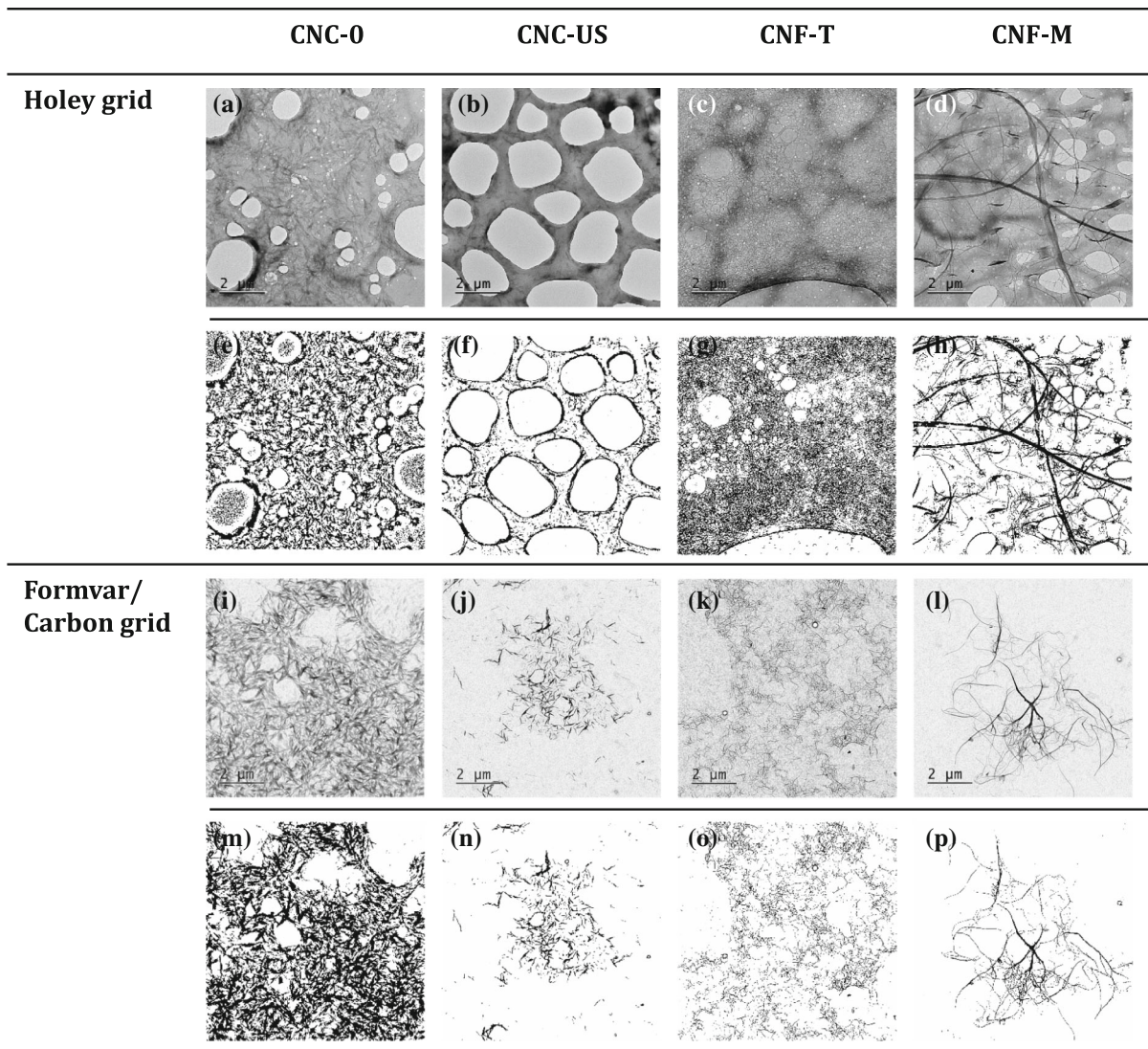


Fig. 1 TEM images of CNCs samples (CNC-0 and CNC-US) and CNFs samples (CNF-T and CNF-M) in the two prepared grids (a–d emulsion/carbon and i–l Formvar/carbon) at $\times 1000$

magnification. Processed images (e–h and m–p) have the same scale as the original ones. Additional larger images of all samples are included in Fig. S5–S12

Results of the TEM image acquisition

An example of the TEM images for the four NC considered is displayed, together with the corresponded treated one, in Fig. 1. In the first row, one can observe the low reproducibility of the preparation on the holey grids, leading to holes of many different sizes and occasionally, some dark areas likely corresponding to incipient holes. In the case of CNCs, typically the diameter of the holes was much larger than the CNCs length, which makes it difficult to

retain this type of NC in this area if they are mostly individualized (Fig. 1a, b). In any case, the presence of irregularities on the covering surface, e.g. the border of the holes of the polymer layer, disrupted the homogeneous deposition of the particles.

On the other hand, there is a very different behavior observed for CNF-T and CNF-M. As observed in Fig. 1c, CNF-T suspension was deposited onto the grid surface building up an interconnected network structure (Han et al. 2019). In this way, it seems that the presence of holes did not affect to the deposition of

the CNF-T. Nevertheless, the high amount of heat generated by the use of high voltages in TEM (Chapman 1986), damaged CNF-T sample deposited on the holes, since without support the heat could not be dissipated in the short time needed to take the image. In the CNF-M, as their length is much higher compared to the size of the holes, the fibers tend to remain in the place they fall during sample preparation, either on the holes or on the polymer covered surface.

As observed in Fig. 1i–l, the sample is not distributed homogeneously on the images taken in the Formvar/carbon grids and neither was it on the whole grid surface. This fact has been explained in the literature to be caused by the layer of evaporated carbon, which provides certain conductivity to the sample, being more hydrophobic (Kaushik et al. 2014). Thus, once the NC is sampled on the grid surface, the particles may tend to aggregate during drying, forming areas of very different concentration over the whole surface (Fig. 1).

As observed in Fig. 1a–d, the edges of the holes limit two areas with much more contrast than the one observed between the NC sample and the polymer covered surface. The contrast in TEM images is affected by electron density of the material and its size (Stinson-Bagby et al. 2018). Since CNCs and CNFs are made mostly of carbon, with low electron density, and have an average diameter between 5 and 20 nm, which is not deep enough for transmitting electrons to interact with the sample, the contrast between CNCs or CNFs and the substrate is commonly a major drawback. (Kaushik et al. 2015b). In addition, at high magnification, the crystallinity of the particles is usually disrupted since they are radiation sensitive, making the lack of contrast in the images more significant. This effect is even more pronounced when the holes are included in the equation. Thus, the isolation of the NC sample during the image treatment becomes challenging in this type of grids, since the borders of the holes remain in the images regardless of the filter applied (Fig. 1e–h).

In the case of the Formvar/carbon coated grids, a more homogeneous surface was observed. In this case, only the sample has a darker color, easing the detection and isolation of either CNCs or CNFs under image analysis. Nevertheless, a dotted background remained in the micrographs, coming from the presence of the two layers deposited on the grids: Formvar

and carbon. The relevance of these dots after sample binarization depends on the image magnification. For $\times 1000$ magnified micrographs, the dots occupy a low proportion of pixels, so they can be easily removed without affecting the size and morphology of the NC sample (Fig. 1i–p). However, for images taken at $\times 5000$ or higher magnification, the dots cover a higher proportion of pixels, and their complete removal from the image is more tedious (Fig. S2).

In all cases, the image analysis of the micrographs taken from the Formvar/carbon grids could be easily automated, taking into account their magnification to adjust the parameters of each filter or plugin. Thus, this type of grid was selected in this study for further analysis of nanocellulosic samples.

Figure 2a–c shows that NC suspensions seems to have been distributed most homogeneously in the images with the use of PLL. This affirmation has been corroborated by the several replicates that have been carried out for each sample, always reaching a similar appearance (Fig. S3). However, the images acquired for CNF-M were quite different among them, probably due to the heterogeneity of this sample in suspension, mainly composed of primary fibers having branches of different diameters. In this case, the use of PLL could provide a better fixing of the nano-hairs that were protruding from the fibers, probably avoiding them attaching back on to the primary fiber and allowing a better visualization of the nanofibers which are still bundled. Moreover, the contrast was not apparently affected by this component, and it was possible to convert images to binary, isolating just the NC sample (Fig. 2e–h).

PLL is a homopolypeptide that contains multiple positively charged hydrophilic amino groups (Ume-hara et al. 2006). Thus, while most of methods used in TEM grids focus on enhancing their hydrophilicity, such as glow discharge or UV radiation, with PLL not only is this much enhanced but also the positive charges allow a more homogeneous deposition of the nanoparticles of anionic nature on the substrate due to electrostatic interactions.

Other authors have pointed for many years to the use of glow discharge or UV radiation in order to achieve a more hydrophilic surface (Areid et al. 2018). Figure 3 shows the images using these two technologies before sample addition. As observed in Fig. 3a–d, sample prepared through glow discharge was not distributed homogeneously over the whole grid.

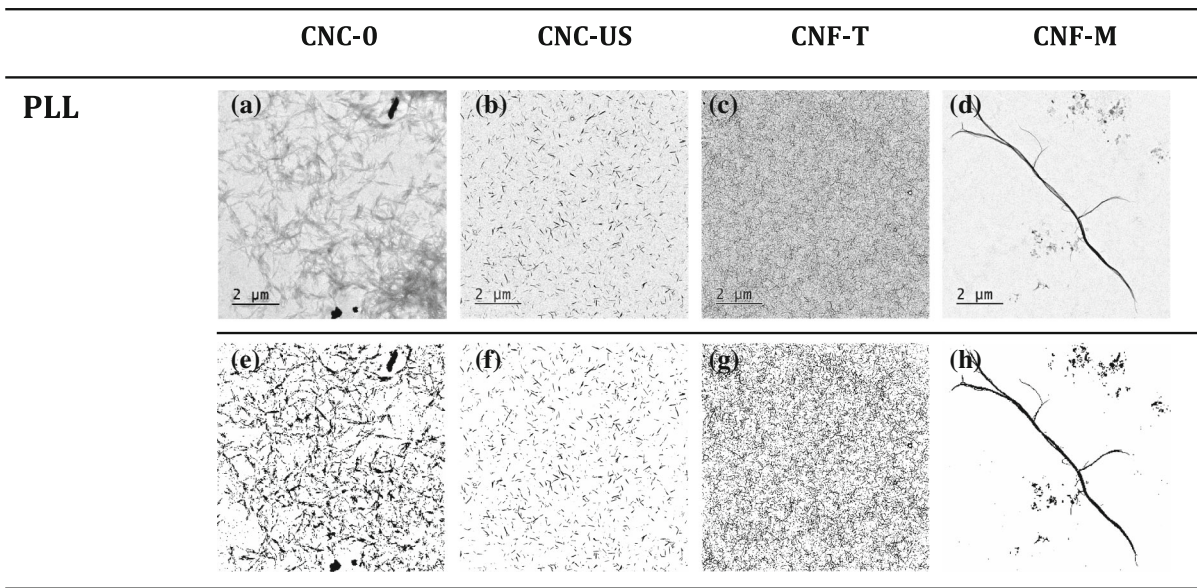


Fig. 2 TEM images of CNCs samples (CNC-0 and CNC-US) and CNFs samples (CNF-T and CNF-M) in the Formvar/carbon grid at $\times 1000$ magnification, with the use of PLL (**a–d**).

Processed images (**e–h**) have the same scale as the original ones. Additional larger images of all samples are included in Fig. S13–S16

Although it was possible to achieve good images of well dispersed sample with this technique, similar to the ones reported before (Brito et al. 2012; Hirota et al. 2010; Kaushik et al. 2015b; Ogawa and Putaux 2019; Saidane et al. 2016), this is not the common pattern (Figure S4), as observed by other authors (Abitbol et al. 2013). Observing the texture of the aggregates of CNCs in Fig. 3a–b, the most probable explanation could be the aggregation of the individual CNCs during drying, since they seem to have a 2D relocation with different group shapes. Commercial systems generally yield negatively charged hydrophilic surfaces (Ogawa and Putaux 2019) that could have caused an extensive aggregation in some areas.

In the case of UV radiation, only images of CNCs were represented, since no CNFs were found in the prepared grids. The main concern regarding the use of UV radiation has been that the irradiation time is rather long and the hydrophilization of carbon is not homogeneous, resulting in patchy negative staining of the nano-objects. This could have been the cause for the low proportion of sample found in the images, especially in the case of CNFs, since they present a network structure. A high heterogeneity was observed in these images, where both CNC-0 and CNC-US were placed only in some areas of the grid, leaving a high proportion of empty places. This observation suggests

that some type of aggregation had likely taken place during sample preparation.

In 2014, Xu et al. demonstrated that the dissociative adsorption of water molecules, observed under UV radiation, induced the wettability transition in carbon surfaces from hydrophobic to hydrophilic. It is also known that this change could be reversible if the treated surface is stored in air. This reversibility could be the cause of the excessively irregular deposition of CNCs v CNCs samples, as observed in Fig. 3.

Reproducibility of the methods: fractal dimension and lacunarity

To justify these preliminary observations, we studied the determination of the fractal dimension and lacunarity of the binary images. The concept of lacunarity is highly scale dependent, so the analyses were carried out of the images at the same scale.

The proportion of sample that was deposited on the grid was measured indirectly through the value of the fractal dimension, while the standard deviation of this parameter indicated the gradient of the concentration on the grid. The way the sample was distributed in the images was quantified through the lacunarity, registering a low value when the sample was distributed homogeneously, and the similarity among the

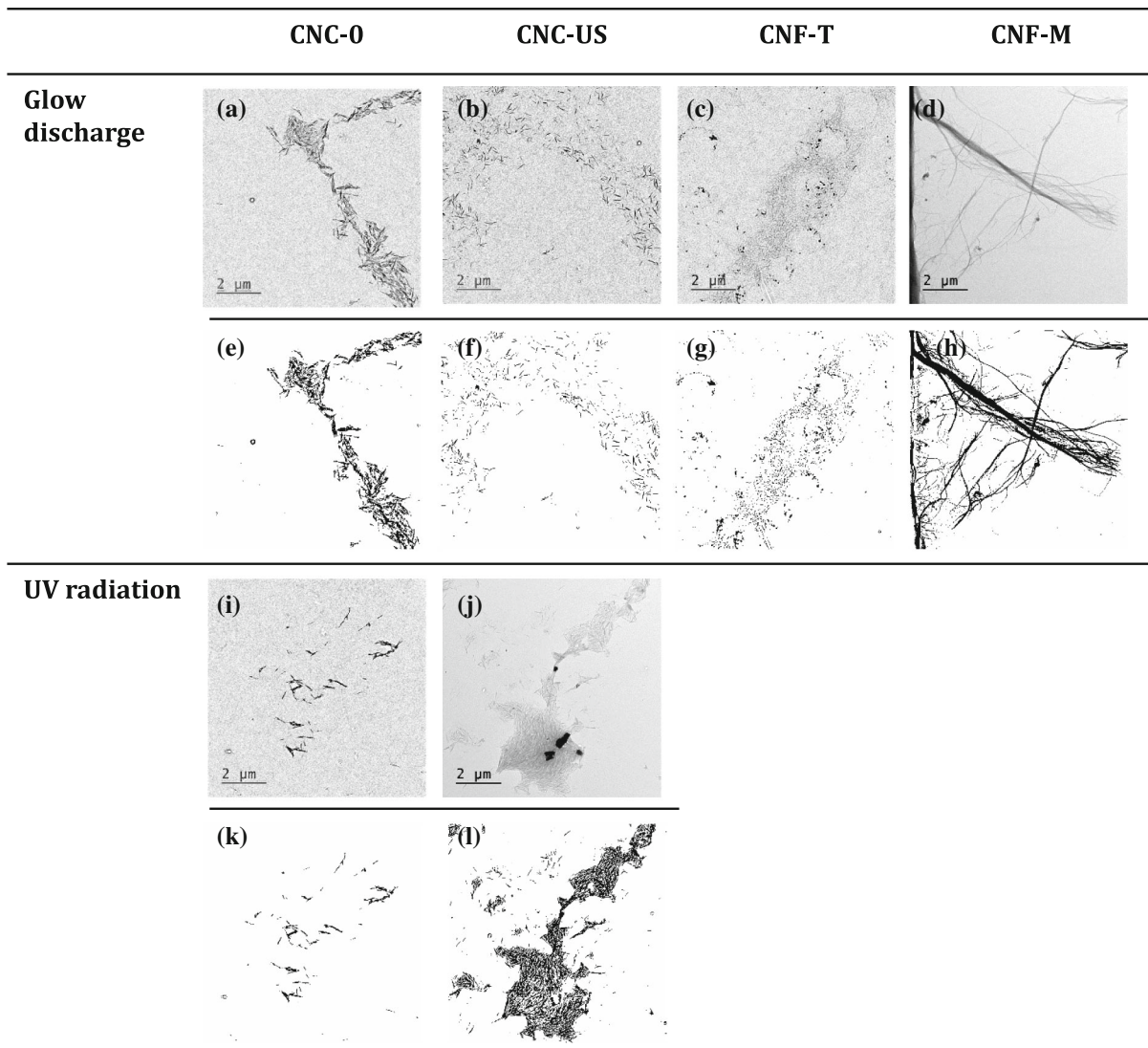


Fig. 3 TEM images ($\times 1000$ magnification) of CNCs and CNFs samples in the Formvar/carbon grid pretreated through glow discharge (a–d) and UV radiation (i–j). Processed images (e–h,

k–l) have the same scale as the original ones. Additional larger images of all samples are included in Fig. S17–S22

different images of the same sample was indicated by the value of the standard deviation of the lacunarity.

CNC-0 and CNC-US were added to the grids at the same concentration and volume. Thus, theoretically, if the sample would have been fixed effectively, the fractal dimension of the images should be the same. Consequently, the lacunarity would have a low value, indicating that most of the gaps present in the images have a homogeneous size.

According to Fig. 4a, fractal dimension of CNC-0 and CNC-US have very different results, with a high

standard deviation of 0.2. Moreover, the lacunarity presents very different values in each analyzed image, with a low value, close to 0.4, in the case of CNC-0 and 1.4 in CNC-US. Since no dispersion method was used in CNC-0, the sample was already in a high aggregation state. Thus, although some aggregation could have occurred during sample drying in the untreated grids, the sample was dispersed quite homogeneously on the substrate, as shown by the low value of lacunarity. However, as this parameter is very sensitive to any change in the size of gaps, the standard

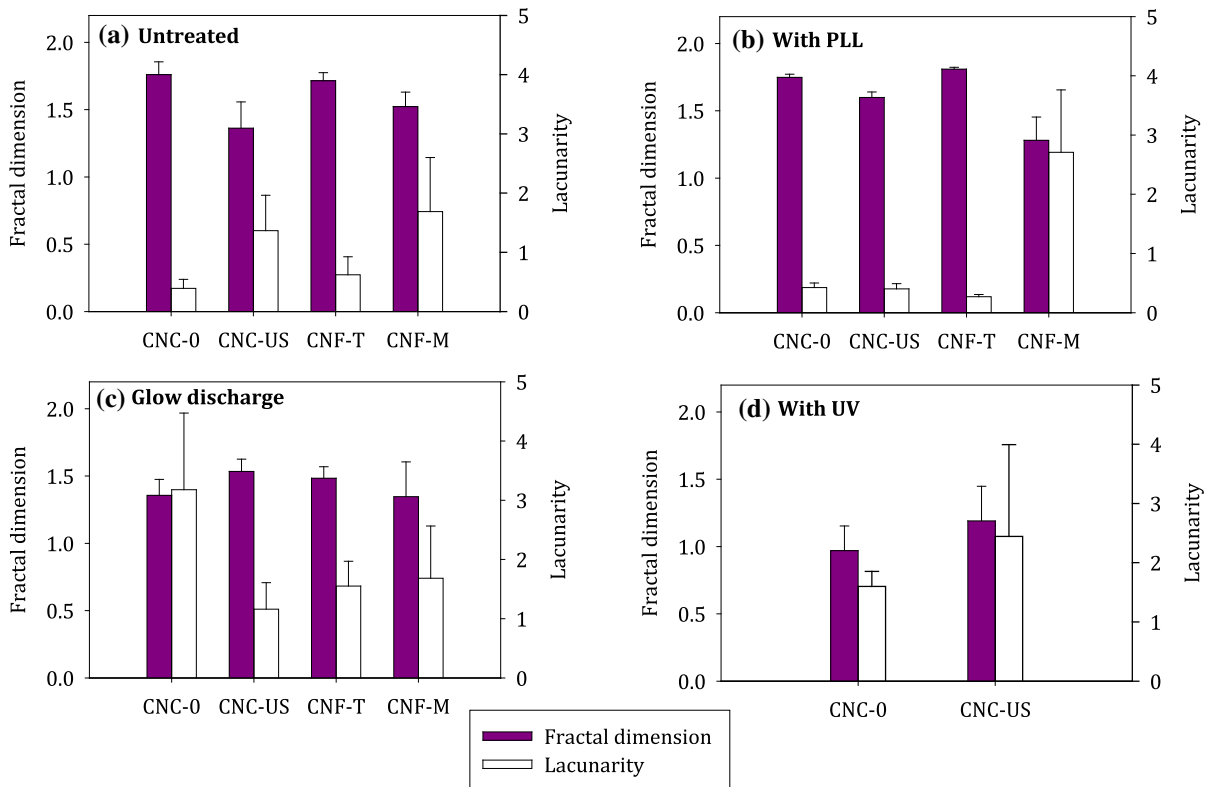


Fig. 4 Fractal dimension and lacunarity results for the NC samples with different fixing agents: **a** Untreated, **b** with PLL, **c** with glow discharge and **d** with UV radiation

deviation indicates that the reproducibility of the image acquisition was probably not very high. Similar results were achieved for CNF-T, even though the concentration of the sample was a tenth of that of CNCs samples.

With the use of PLL as fixing agent, the fractal dimension of CNC-0, CNC-US and CNF-T was very similar for each of them, with a very low standard deviation and a very homogeneous distribution, as shown by the low value of lacunarity. Low concentrations of NC samples, as in this case, would present a relatively low overlapping when deposited on a surface. Given that aggregates of CNCs particles are ensembles of geometrically similar individual units, the images of homogeneously deposited, low concentrated samples would be expected to present very similar average fractal dimensions. On the other hand, the fact that fractal dimension of CNF-T was very similar to that of CNCs samples, even though CNF-T was sampled at half of the concentration of CNCs, was probably due to the more interconnected network that

CNF-T has, allowing a higher deposition than that achieved by CNCs.

Fractal dimension results obtained with the glow discharge technique (Fig. 4c), presented very similar values among all prepared samples, but lower than those achieved with the previous methods (the untreated grids and the treated with PLL). This indicated a lower deposition, probably due to the negative hydrophilization of the grids, which repelled a proportion of the sample from the substrate. On the other hand, the high values of lacunarity observed in the graph were quite striking, indicating a high irregularity in the sample distribution, as observed in Fig. S4.

Finally, in the case of UV, a low proportion of sample was found in the images, as shown in Fig. 3, which corresponded to a low value of fractal dimension, observed in Fig. 4d. In addition, the distribution of the sample in the micrographs was much more irregular than in the rest of the samples (in the untreated grids and the ones with PLL), as shown by

the values of lacunarity, and a low reproducibility was shown in the method, as indicated by the standard deviation of the lacunarity.

In the case of CNF-M, very different results were observed, showing a lower fractal dimension of around 1.5, with a higher standard deviation. This shows that the amount of sample presented in each image is low and very irregular in each one. The high heterogeneity of the sample is probably the cause of the irregular sample deposition on the grids, and it is associated with high lacunarity values with large standard deviations.

Hence, the preliminary conclusion of the previous section has been corroborated by these observations: with the use of PLL, the sample is distributed homogeneously on the grid, and the replication of the test provides reproducible results. From this study we could conclude that the use of PLL in sample preparation is useful to fix the sample to the substrate, providing a high reproducibility on the image acquisition and easing the subsequent image interpretation. In addition, the use of fractal dimension and lacunarity was very useful to quantify the reproducibility of the methods as long as the sample is mostly homogeneous.

Effect of negative staining

The use of staining agents in order to increase the contrast of the nanoparticles in the images is a common practice among researchers in this field (Stinson-Bagby et al. 2018). It has been proved that the negative staining of NC provides accurate measurements of their individual size (Kvien et al. 2005). However, the most common agent used for this purpose, uranyl acetate, is a relatively expensive and toxic heavy metal salt, and sometimes is related to some aggregation problems in the drying step (Cirtiu et al. 2011).

However, the use of negative staining to further increase contrast could interfere with the PLL, so these interactions were investigated, and the images were shown in Fig. 5. Although the same procedure was used for all the samples, only the negative staining was achieved for CNC-0 without PLL (Fig. 5a), while the rest of the samples presented a positive staining.

On the other hand, from Fig. 5i–l, many artefacts remained in the substrate when PLL and uranyl acetate were used simultaneously, in addition creating dirty areas of different contrast that remained even after

image treatment. Due to the nature of both components, being of positive charge, it is highly probable that uranyl acetate was repelled by the layer of PLL, creating some drops that appear in the images with a contrast similar that of the NC. The quality of these images is, therefore, very poor, and, consequently, their analysis is unreliable.

To check the effect of the use of sample staining in the image analysis, fractal dimension and lacunarity were also calculated from treated images with and without PLL addition (Fig. 6). In the case of the grids prepared without PLL, the fractal dimension of the samples remained almost unchanged with the use of negative staining. However, a low proportion of the impurities in the images triggered a high change in the lacunarity. Comparing the values of lacunarity plotted in Figs. 6a and 4a, only that of CNC-US was increased (from 1.3 to 2.0), indicating a higher dispersion in the size of the gaps. It is possible that the staining of the sample would have been more heterogeneous in this case due to the closeness of CNCs particles. It has been observed in some of the micrographs that when two particles were very close, the area between them is stained, filling this gap and, therefore, breaking the homogeneity of the black areas in the binary images.

In the case of the images obtained with the covering of the grid with PLL prior to sample preparation, fractal dimension was again found almost unchanged. In this case, despite the presence of artefacts identified in the images (Fig. 5i–l), the values of lacunarity were very similar among them. This indicated that these impurities were likely distributed very homogeneously over the substrate, forming smaller gaps but of very similar size. Only in the CNF-M, was a decrease in the lacunarity observed. It is possible that the artefacts decreased the difference in size among the gaps, thus getting a lower value of lacunarity.

To assess the effect of negative staining on the morphology of NC, the diameter of individual particles was measured and the results were plotted in Fig. 7. The diameter determined for the stained CNC-0 was lower than that unstained, which corresponded to the better imaging of the limits of the CNCs, allowing a more accurate measurement. Nevertheless, the filling of the small areas present in the CNC-US, CNF-T and CNF-M with the positive staining, could have increased the difficulty in detecting the borders of the CNCs, thus increasing the measured diameter.

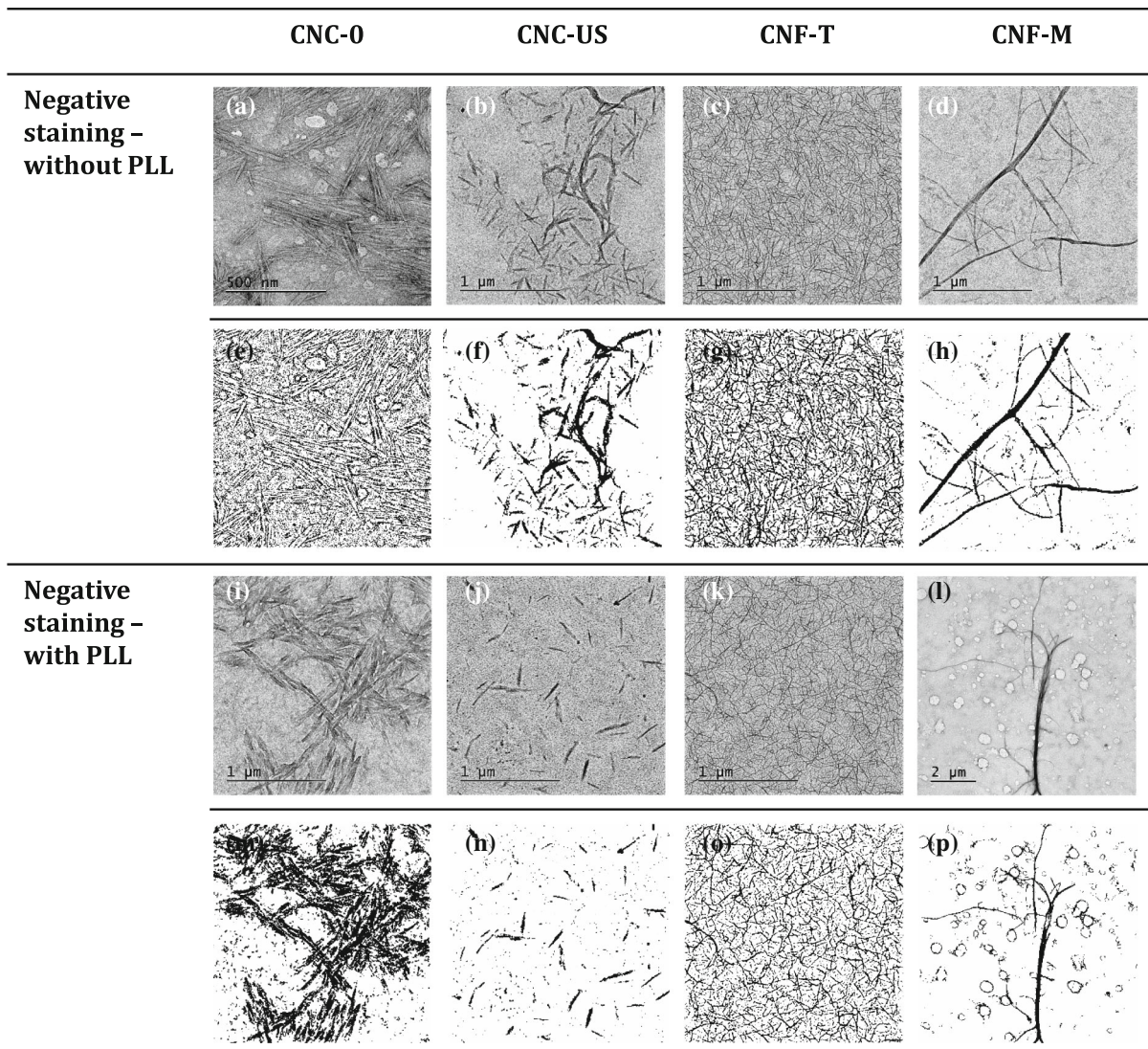


Fig. 5 TEM images of CNCs samples (CNC-0 and CNC-US) and CNFs samples (CNF-T and CNF-M) in the Formvar/carbon grid using negative staining (without (a–d) and with PLL (i–l)).

Processed images (e–h and m–p) have the same scale as the original ones. Additional larger images of all samples are included in Fig. S23–S30

On the other hand, Fig. 7b shows that there is a high heterogeneity in the results obtained with the use of PLL. Again, the staining agent acts in a different way each time it is used, due to its interactions with PLL. Thus, in some cases, the diameter of the NCs is increased, maybe pointing to a positive staining and, in others, it is slightly decreased, probably because of the failing action of the methodology.

As the stained samples have a higher diameter than the unstained ones (considering the stain plus the nanoparticles), it is quite difficult to remove this effect

when performing image analysis. Thus, the use of negative staining should be considered when one only intends to highlight the morphology of individual particles, including size and shape, and not trying to describe the bulk morphology of CNCs or CNFs.

Conclusions

This study demonstrates a new methodology to analyze the bulk morphology or 3D structure of NC

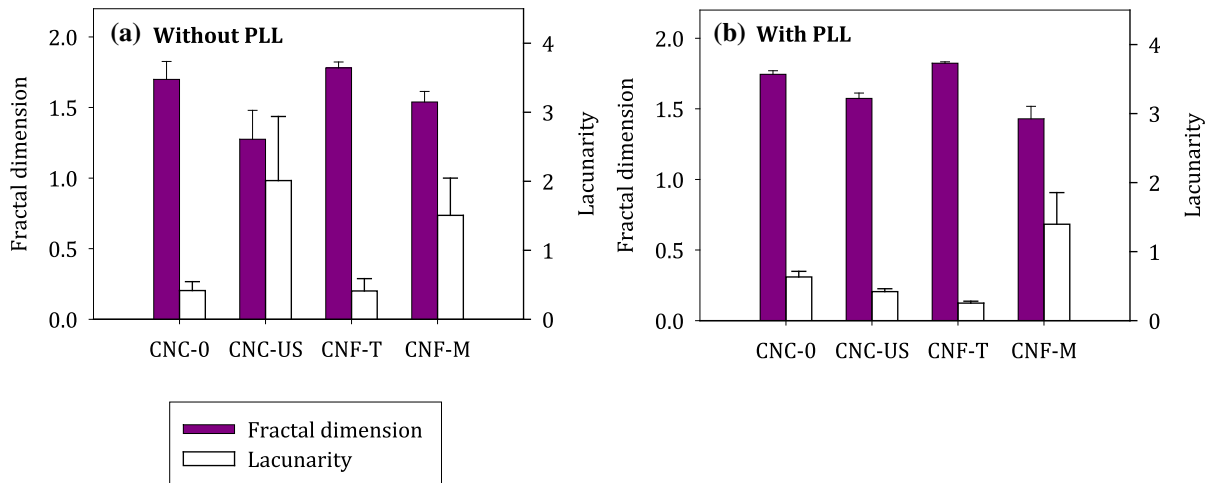


Fig. 6 Fractal dimension and lacunarity of the stained samples **a** with the untreated grid and **b** with the grid treated with PLL

in suspension using TEM. With the high reproducibility observed in the images, it can be concluded that the initial state of the NC in suspension can be accurately characterized by TEM with further image analysis.

Both types of grids used in this study allowed the identification of NC samples. However, Formvar/carbon coated grids provided a higher and more uniform contrast than the holey grids. In addition, the distribution of the sample over the whole surface was more homogenous since no irregularities influenced the NC deposition.

Fractal dimension and lacunarity, measured in the images, were found to be important in order to quantify the reproducibility of the methods. The distribution of the NC sample was much more

homogeneous when PLL was used as fixing agent of NC. With the coating of the grid using PLL prior to sample deposition, the highly fibrillated NC, namely CNC-0, CNC-US and CNF-T, were placed homogeneously, as shown by the low values of lacunarity. The reproducibility of this method was very high as indicated by the low standard deviation of the lacunarity. However, the use of negative staining did not provide any improvement in the image contrast, since uranyl acetate and PLL interacted, forming artefacts that corrupted the interpretation of the sample.

PLL induced very improved results compared with the traditionally used glow discharge, due to the fact that not only hydrophilicity was increased, but also the

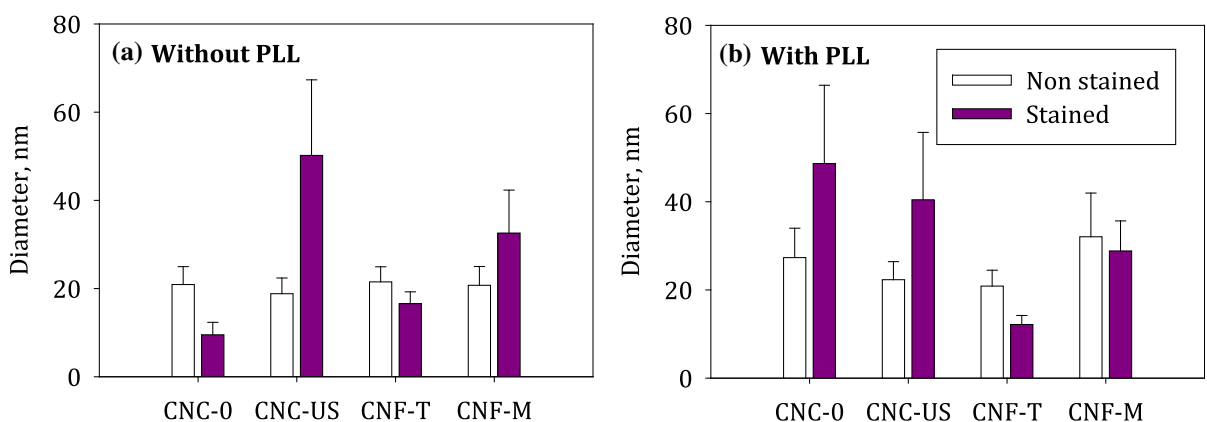


Fig. 7 Diameter of individual nanocelluloses measured without staining and stained in **a** untreated grids and **b** grids treated with PLL

cationic character of PLL allowed a homogeneous and durable fixing of the sample of anionic nature. Thus, with the use of PLL on Formvar/carbon grids, one could ensure that the bulk morphology of NC suspensions could be described through the analysis of TEM images. This approach points to a very promising method for an online characterization of some geometrical parameters, such as the aggregation/dispersion degree of CNCs and the nanofibrillation degree of CNFs samples. Moreover, this method could be extended to the characterization of the 3D structure of other nanoparticles of anionic nature.

Acknowledgments Authors want to acknowledge the Spanish Ministry of Economy and Competitiveness for the funding of the project CTQ2017-85654-C2-2-R, as well as the Community of Madrid for funding the RETO-PROSOST-2-CM (P2018/EMT4459). Also thanks to the Spanish National Centre of Electronic Microscopy for the support during image acquisition. Authors also want to thank Laura González Aguilera for the help in the experimental work.

References

- Abitbol T, Kloser E, Gray DG (2013) Estimation of the surface sulfur content of cellulose nanocrystals prepared by sulfuric acid hydrolysis. *Cellulose* 20:785–794
- Araki J (2013) Electrostatic or steric? Preparations and characterizations of well-dispersed systems containing rod-like nanowhiskers of crystalline polysaccharides. *Soft Matter* 9:4125–4141. <https://doi.org/10.1039/C3SM27514K>
- Areid N, Peltola A, Kangasniemi I, Ballo A, Närhi TO (2018) Effect of ultraviolet light treatment on surface hydrophilicity and human gingival fibroblast response on nanostructured titanium surfaces. *J Clin Exp Dent* 4:78–85. <https://doi.org/10.1002/cre2.108>
- Arias A, Heuzey M-C, Huneault MA, Ausias G, Bendahou A (2015) Enhanced dispersion of cellulose nanocrystals in melt-processed polylactide-based nanocomposites. *Cellulose* 22:483–498. <https://doi.org/10.1007/s10570-014-0476-z>
- Balea A, Merayo N, Fuente E, Delgado-Aguilar M, Mutje P, Blanco A, Negro C (2016a) Valorization of corn stalk by the production of cellulose nanofibers to improve recycled paper properties. *BioResources* 11:3416–3431
- Balea A, Merayo N, Fuente E, Negro C, Blanco A (2016b) Assessing the influence of refining, bleaching and TEMPO-mediated oxidation on the production of more sustainable cellulose nanofibers and their application as paper additives. *Ind Crops Prod* 97:374–387. <https://doi.org/10.1016/j.indcrop.2016.12.050>
- Beck S, Méthot M, Bouchard J (2015) General procedure for determining cellulose nanocrystal sulfate half-ester content by conductometric titration. *Cellulose* 22:101–116. <https://doi.org/10.1007/s10570-014-0513-y>
- Brinkmann A, Chen MH, Couillard M, Jakubek ZJ, Leng TY, Johnston LJ (2016) Correlating cellulose nanocrystal particle size and surface area. *Langmuir* 32:6105–6114. <https://doi.org/10.1021/acs.langmuir.6b01376>
- Brito BS, Pereira FV, Putaux J-L, Jean B (2012) Preparation, morphology and structure of cellulose nanocrystals from bamboo fibers. *Cellulose* 19:1527–1536
- Campano C, Miranda R, Merayo N, Negro C, Blanco A (2017) Direct production of cellulose nanocrystals from old newspapers and recycled newsprint. *Carbohydr Polym* 173:489–496. <https://doi.org/10.1016/j.carbpol.2017.05.073>
- Chapman SK (1986) Maintaining and monitoring the transmission electron microscope, vol 8. Oxford University Press, Oxford
- Chen W et al (2015) Revealing the structures of cellulose nanofiber bundles obtained by mechanical nanofibrillation via TEM observation. *Carbohydr Polym* 117:950–956. <https://doi.org/10.1016/j.carbpol.2014.10.024>
- Cherhal F, Cousin F, Capron I (2015) Influence of charge density and ionic strength on the aggregation process of cellulose nanocrystals in aqueous suspension, as revealed by small-angle neutron scattering. *Langmuir* 31:5596–5602. <https://doi.org/10.1021/acs.langmuir.5b00851>
- Chinga-Carrasco G, Yu Y, Diserud O (2011) Quantitative electron microscopy of cellulose nanofibril structures from eucalyptus and *Pinus radiata* kraft pulp fibers. *Microsc Microanal* 17:563–571. <https://doi.org/10.1017/S1431927611000444>
- Cirtiu CM, Dunlop-Briere AF, Moores A (2011) Cellulose nanocrystallites as an efficient support for nanoparticles of palladium: application for catalytic hydrogenation and Heck coupling under mild conditions. *Green Chem* 13:288–291. <https://doi.org/10.1039/COGC00326C>
- Dufresne A (2012) Preparation of cellulose nanocrystals. Nanocellulose: from nature to high performance tailored materials. Walter de Gruyter, Germany, pp 117–175
- Dulińska I, Targosz M, Strojny W, Lekka M, Czuba P, Balwierz W, Szymoński M (2006) Stiffness of normal and pathological erythrocytes studied by means of atomic force microscopy. *J Biochem Biophys Meth* 66:1–11. <https://doi.org/10.1016/j.jbbm.2005.11.003>
- Elazzouzi-Hafraoui S, Nishiyama Y, Putaux J-L, Heux L, Dubreuil F, Rochas C (2007) The shape and size distribution of crystalline nanoparticles prepared by acid hydrolysis of native cellulose. *Biomacromolecules* 9:57–65. <https://doi.org/10.1021/bm700769p>
- Fall AB, Lindström SB, Sundman O, Ödberg L, Wågberg L (2011) Colloidal stability of aqueous nanofibrillated cellulose dispersions. *Langmuir* 27:11332–11338. <https://doi.org/10.1021/la201947x>
- Habibi Y, Chanzy H, Vignon MR (2006) TEMPO-mediated surface oxidation of cellulose whiskers. *Cellulose* 13:679–687. <https://doi.org/10.1007/s10570-006-9075-y>
- Han X, Ye Y, Lam F, Pu J, Jiang F (2019) Hydrogen-bonding-induced assembly of aligned cellulose nanofibers into ultrastrong and tough bulk materials. *J Mater Chem A* 7:27023–27031. <https://doi.org/10.1039/C9TA11118B>
- Henriksson M, Berglund LA, Isaksson P, Lindstrom T, Nishino T (2008) Cellulose nanopaper structures of high toughness.

- Biomacromolecules 9:1579–1585. <https://doi.org/10.1021/bm800038n>
- Hirota M, Tamura N, Saito T, Isogai A (2010) Water dispersion of cellulose II nanocrystals prepared by TEMPO-mediated oxidation of mercerized cellulose at pH 48. *Cellulose* 17:279–288
- Kaech S, Banker G (2006) Culturing hippocampal neurons. *Nat Protoc* 1:2406. <https://doi.org/10.1038/nprot.2006.356>
- Kaushik M, Chen WC, van de Ven TG, Moores A (2014) An improved methodology for imaging cellulose nanocrystals by transmission electron microscopy. *Nord Pulp Paper Res J* 29:77–84. <https://doi.org/10.3183/npprj-2014-29-01-p077-084>
- Kaushik M, Basu K, Benoit C, Cirtiu CM, Vali H, Moores A (2015a) Cellulose nanocrystals as chiral inducers: enantioselective catalysis and transmission electron microscopy 3D characterization. *J Am Chem Soc* 137:6124–6127. <https://doi.org/10.1021/jacs.5b02034>
- Kaushik M, Fraschini C, Chauve G, Putaux J-L, Moores A (2015b) Transmission electron microscopy for the characterization of cellulose nanocrystals. In: Maaz K (ed) *The transmission electron microscope. Theory and applications*. InTech, Croatia, pp 129–164
- Klemm D et al (2018) Nanocellulose as a natural source for groundbreaking applications in materials science: Today's state. *Mater Today* 21:720–748. <https://doi.org/10.1016/j.mattod.2018.02.001>
- Kvien I, Tanem BS, Oksman K (2005) Characterization of cellulose whiskers and their nanocomposites by atomic force and electron microscopy. *Biomacromolecules* 6:3160–3165. <https://doi.org/10.1021/bm050479t>
- Mohraz A, Moler DB, Ziff RM, Solomon MJ (2004) Effect of monomer geometry on the fractal structure of colloidal rod aggregates. *Phys Rev Lett* 92:155503. <https://doi.org/10.1103/PhysRevLett.92.155503>
- Ogawa Y, Putaux J-L (2019) Transmission electron microscopy of cellulose. Part 2: technical and practical aspects. *Cellulose* 26:17–34
- Reichert R, König T, Wangermann G (1977) Preparation of microgrids as specimen supports for high resolution electron microscopy. *Micron* 8:29–31. [https://doi.org/10.1016/0047-7206\(77\)90005-X](https://doi.org/10.1016/0047-7206(77)90005-X)
- Reiss MA, Lemmerer B, Hanslmeier A, Ahammer H (2016) Tug-of-war lacunarity—a novel approach for estimating lacunarity. *Chaos* 26:113102. <https://doi.org/10.1063/1.4966539>
- Riddick TM (1968) *Control of colloid stability through zeta potential*. Livingston Wynnewood, USA
- Saidane D, Perrin E, Cherhal F, Guellec F, Capron I (2016) Some modification of cellulose nanocrystals for functional Pickering emulsions. *Philos Trans R Soc A* 374(2072):20150139
- Saito T, Kimura S, Nishiyama Y, Isogai A (2007) Cellulose nanofibers prepared by TEMPO-mediated oxidation of native cellulose. *Biomacromolecules* 8:2485–2491. <https://doi.org/10.1021/bm0703970>
- Sanchez-Salvador JL, Monte MC, Batchelor W, Garnier G, Negro C, Blanco A (2020) Characterizing highly fibrillated nanocellulose by modifying the gel point methodology. *Carbohydr Polym* 227:115340. <https://doi.org/10.1016/j.carbpol.2019.115340>
- Segal L, Creely JJ, Martin AE, Conrad CM (1959) An empirical method for estimating the degree of crystallinity of native cellulose using the X-ray diffractometer. *Text Res J* 29:786–794. <https://doi.org/10.1177/004051755902901003>
- Stinson-Bagby KL, Roberts R, Foster EJ (2018) Effective cellulose nanocrystal imaging using transmission electron microscopy. *Carbohydr Polym* 186:429–438. <https://doi.org/10.1016/j.carbpol.2018.01.054>
- Uhlig M et al (2016) Two-dimensional aggregation and semidilute ordering in cellulose nanocrystals. *Langmuir* 32:442–450. <https://doi.org/10.1021/acs.langmuir.5b04008>
- Umehara S, Pourmand N, Webb CD, Davis RW, Yasuda K, Karhanek M (2006) Current rectification with poly-L-lysine-coated quartz nanopipettes. *Nano Lett* 6:2486–2492
- Wang QQ, Zhu JY, Reiner RS, Verrill SP, Baxa U, McNeil SE (2012) Approaching zero cellulose loss in cellulose nanocrystal (CNC) production: recovery and characterization of cellulosic solid residues (CSR) and CNC. *Cellulose* 19:2033–2047. <https://doi.org/10.1007/s10570-012-9765-6>
- Xu Z, Ao Z, Chu D, Younis A, Li CM, Li S (2014) Reversible hydrophobic to hydrophilic transition in graphene via water splitting induced by UV irradiation. *Sci Rep* 4:6450. <https://doi.org/10.1038/srep06450>
- Yang H, Chen DZ, van de Yen TGM (2015) Preparation and characterization of sterically stabilized nanocrystalline cellulose obtained by periodate oxidation of cellulose fibers. *Cellulose* 22:1743–1752. <https://doi.org/10.1007/s10570-015-0584-4>
- Young K, Morrison H (2018) Quantifying microglia morphology from photomicrographs of immunohistochemistry prepared tissue using ImageJ. *J Vis Exp*. <https://doi.org/10.3791/57648>

Publisher's Note Springer Nature remains neutral with regard to jurisdictional claims in published maps and institutional affiliations.